

Multi-channel Kondo effect in finite lattices
(Mehrkanal Kondo-Effekt in endlichen Gittern)

von

Yannick Couzinié

geboren am

11. Juni 1995

Bachelor-Arbeit im Studiengang Physik

Universität Hamburg

2016

1. Gutachter: Prof. Dr. Michael Potthoff
2. Gutachter: Prof. Dr. Michael Thorwart

Abstract

A first-order perturbative approach to the Kondo model in the low energy scale ($T = 0$) for nanoscale systems is presented. The coupling between any amount of magnetic impurities, modelled as quantum spins, and spin orbitals in a metallic lattice can be anisotropic and both local and non-local. While the lattice dimension and geometry can be chosen freely, the Fermi energy level needs to be incompletely occupied. The result is an effective coupling model, giving control over the distinction between under-, complete and overscreening. Numerical calculations on exemplary one-dimensional systems are then evaluated and briefly discussed, one of which is a system frequently used to discuss and measure overscreening.

Zusammenfassung

Ein Ansatz erster Ordnung Störungstheorie, angewendet auf das Kondo Modell bei geringen Energien ($T = 0$) für nanoskopische Systeme, wird vorgestellt. Die Kopplung kann anisotrop, lokal und nicht-lokal zwischen einer beliebigen Anzahl an magnetischen Verunreinigungen, modelliert als Quantenspins, und Spinorbitalen eines metallischen Gitters sein. Während die Dimension und Geometrie des Gitters frei wählbar ist, muss das Fermi-Niveau unvollständig besetzt sein. Als Ergebnis erhält man ein effektives Kopplungsmodell, welches eine einfache Unterscheidung zwischen Under-, complete, und Overscreening erlaubt. Numerische Berechnungen zu beispielhaften eindimensionalen Systemen werden präsentiert und diskutiert, wobei eines der Systeme häufig zur Diskussion und Messung des Overscreenings verwendet wird.

Contents

1. Introduction	1
2. Non-local, anisotropic coupling of multiple impurities to a finite lattice	5
2.1. Model	5
2.2. Numerical results	11
2.2.1. One Fermi electron	15
2.2.2. Two Fermi electrons	17
3. Forced overscreening	25
3.1. Set-up	25
3.2. Numerical results	26
4. Conclusions and Outlook	31
A. One dimensional systems with periodic boundary conditions	35
B. Choosing the sign for the coupling constant	37

1. Introduction

A paper published in 1934 [1], which presented measurements in which the electrical resistivity of metals increased with decreasing temperatures, dumbfounded physicists upon its release. Relying mainly on phonon scattering as an explanation for electrical resistivity for lower temperatures, the resistivity was expected to decrease monotonically with the temperature as the phonon modes froze [2]. The observation of a resistivity minimum in metals was in stark conflict with this view and the search for a new physical principle explaining the measurement began.

It was not until 1964 that an explanation was published by J. Kondo [3]. Kondo modelled the magnetic impurity in the metal as a quantum spin, which couples via an exchange interaction J to the spin of the conduction electrons in the metal, in the thermodynamic limit. Using third order perturbation theory in J , he derived an $\ln T$ contribution to the resistivity, which, for anti-ferromagnetic J at low temperatures, increases faster than the phonon modes freeze [4].

Having explained the measurement, the publication gave rise to new a problem. Because the contribution diverges for $T \rightarrow 0$, it was clear that Kondo's perturbative approach was not applicable for low temperatures. In fact there is an energy scale, known as the Kondo temperature $T_K \sim e^{-1/J}$, below which a non-perturbative explanation was necessary. This is generally known as the Kondo problem.

The theoretical solution was first qualitatively found by Anderson with his *poor man's scaling* approach [5], then non-perturbatively by Wilson with his *numerical renormalization group* [6], which was confirmed by an ansatz as a Landau Fermi liquid given by Nozières [7] and finally it was solved exactly by Andrei [8] and Wiegmann [9] using the Bethe ansatz. It was shown that for very low energy scales $T \ll T_K$, the coupling strength increases indefinitely, as the energy scale is reduced. This implied a singlet being formed

1. Introduction

by the impurity spin and conduction electron spins in a spatially extended wave function. The impurity is thus effectively screened by the orbital spins of the metallic lattice, over which the wave function extends, usually referred to as the screening cloud [10]. The spatial extension of the screening cloud is given by $\xi_K = \frac{\hbar v_F}{k_B T_K}$, with the Fermi-velocity v_F (\hbar and k_B shall henceforth be set to 1) and is usually estimated to be of the magnitude $0.1 - 1\mu m$.

While the Kondo model has attracted great theoretical and experimental interest, especially during the search for a solution to the Kondo problem and recently again, it is actually implied in the Anderson model [11], which takes impurity states and Coulomb-interaction between conduction electrons into account. The fact that the latter model implies the former has been shown by Schrieffer and Wolf [12], in which they show that an Anderson model with impurities forming a local magnetic moment, was equivalent to the Kondo model. It is because of the varied ways this local magnetic moment can be used, that the Kondo model still keeps being a field of interest in condensed matter research. The research topics are diverse, ranging from heavy fermion physics, where electrons with an effective mass of up to $10^3 m_e$ display Kondo-like Fermi liquid physics [4], over Quantum dots, in which Kondo-like Fermi liquid physics lead to a minimum in the conductance for finite temperatures [13–15] to topological systems like Kondo insulators [16, 17] and superconductors [18] amongst other topics.

A noteworthy property of the Kondo model is that upon transitioning to a system with length scales below the spatial extension of the screening cloud, the thermodynamic limit is no longer applicable and a new approach to solve the Kondo problem is necessary [19–22]. The Kondo model for nanoscale systems is known as the Kondo box [19] and measurements have been realized in metal grains [23–25] and carbon nanotubes [26, 27]. Remarkably, as one leaves the thermodynamic limit, perturbation theory for these Kondo Boxes gives results which are evaluable even in the low energy scales $T \ll T_K$. Using this feature of Kondo boxes, it is possible to give accurate descriptions of the competition between inter-impurity interaction, due to the Ruderman-Kittel-Kasuya-Yosida (RKKY) interaction [28–30], and the Kondo effect [31, 32]. Moreover, thorough analyses of the conduction electron orbital structures and their influences on the screening effectiveness of multiple impurities [32, 33] are possible. At the same time, a new energy scale is introduced in the

form of the now finite gap energies ΔE which leads to new regimes, for example spin-flip scattering for ΔE greater than the Kondo temperature T_K [32].

While the perturbative approach presented in Ref. [32] has been shown to work well for the description of multi-impurity systems, it has failed to describe the case of multiple electrons trying to screen one impurity, i.e. multi-channel systems. These systems were first proposed by Nozières and Blandin in Ref. [34], in which they were assumed to occur in real metals. Since then an adequate description in the mesoscopic Kondo model has been given [35,36]. As such it is desirable to find an equivalent description for nanoscale systems. Nozières identified three regimes that could occur [37]: *Underscreening*, when there are less screening channels available than impurities, thus leading to incompletely screened impurities, *complete screening*, when each impurity spin is completely screened by exactly one conduction electron spin, corresponding to a non-magnetic ground state, and *overscreening*, when there are more screening channels available than impurities, leading to a degeneracy in the ground state as the impurity spin has no preference for a screening channel, i.e. a magnetic ground state. It is the latter case of overscreening, that has not been described by previous theoretical discussions in the perturbative approach for Kondo boxes [32]. All the while, amongst other things because it displays non-Fermi liquid physics [34,37–39], the effect of overscreening has gathered great theoretical interest e.g. in relation to topological superconductors [40], topological Kondo insulators [41], or graphene [42]. Furthermore, experimental realizations of an overscreened impurity have been made [43–45].

The theory presented in this thesis aims to fill this gap between the description of Kondo boxes and the possible screening regimes in the low energy scale.

By including anisotropic, local and non-local coupling between a freely selectable amount of impurities modelled as quantum spins and spin orbitals in a lattice of arbitrary dimension and geometry and applying first-order perturbation theory in J , one finds an effective model in which delocalized spin orbitals of the metal couple to the spins of the impurities. The effective model found has the significant property of easily distinguishing between the three screening regimes.

The derivation of the effective model in Sec. 2.1 is followed by an exemplary analysis of one-dimensional, single impurity systems in Sec. 2.2. It will be shown that overscreening

1. Introduction

is adequately described by this theory. Furthermore, a set-up, similar to the one used in Ref. [43] for measurements, or in Ref. [39] for theoretical discussions, referred to as *forced overscreening* in this thesis, is discussed theoretically and numerically in Sec. 3.1 and 3.2 respectively.

2. Non-local, anisotropic coupling of multiple impurities to a finite lattice

This Sec. will treat the case of impurities non-locally coupling to a single finite lattice with nanoscale lengths, i.e. the case of a Kondo Box. The term non-local coupling is used to refer to local and n th order next-neighbour coupling with $n \in \mathbb{N}$. It begins with the mathematical and perturbative discussion of the Model in Sec. 2.1 and continues with the discussion of numerical results for two exemplary one-dimensional systems in Sec. 2.2. The discussions are in the low energy scale, which refers to temperatures well below the gap energies ΔE and Kondo temperature T_K , this ensures no phase transitions out of the Kondo regime. Furthermore, the gap energies are also assumed to be smaller than the Kondo temperature to avoid suppressions of the Kondo effect [32], i.e. $T \ll \Delta E \ll T_K$.

2.1. Model

The starting point is a modified Kondo Hamiltonian, such that there is a perturbation H_1 describing multi-channel, multi-impurity and anisotropic bindings of impurities to conduction electrons,

$$H = H_0 + H_1 = \sum_{jj'\sigma} t_{jj'} c_{j\sigma}^\dagger c_{j'\sigma} + \sum_{r=1}^R \sum_{n=1}^L \sum_{\alpha}^{\{x,y,z\}} J_{nr}^{(\alpha)} s_n^{(\alpha)} S_{ir}^{(\alpha)}. \quad (2.1.1)$$

H_0 is the Hamiltonian of the unperturbed system, consisting of N non-interacting conduction electrons in a lattice with L sites, with their respective spin orbitals $|j, \sigma\rangle$ at each site $j \in \{1, \dots, L\}$, between which there is a hopping $t_{jj'}$. $c_{j\sigma}^\dagger$ is the creation and $c_{j\sigma}$ the annihilation operator for a spin in the j th orbital with a spin component in the z -direction of σ , i.e. \uparrow or \downarrow . For later calculations one has to impose the restriction on the hopping

2. Non-local, anisotropic coupling of multiple impurities to a finite lattice

matrix $t_{jj'}$ that it is diagonalizable through unitary transformation.

The free system is perturbed by the Hamiltonian H_1 , describing coupling between conduction electrons and impurities modelled as quantum spins, whereby $s_n^{(\alpha)}$ is the α component of the conduction electron spin density at the n th lattice site, with $n \in \{1, \dots, L\}$ and $S_{i_r}^{(\alpha)}$ the α component of the r th impurity spin, where i_r denotes the lattice site to which it couples locally. The spin reads in the second quantization formalism as follows: $\mathbf{s}_n = \frac{1}{2} \sum_{\sigma\sigma'} c_{n,\sigma}^\dagger \boldsymbol{\sigma}_{\sigma\sigma'} c_{n\sigma'}$, whereby \mathbf{s} is the spin vector and $\boldsymbol{\sigma}$ the vector of Pauli matrices. The coupling strength between the α component of the n th orbital and the r th impurity spin is governed by the coupling strength matrix $J_{ni_r}^{(\alpha)}$. The notation of H_1 is schematically illustrated in Fig. 2.1.

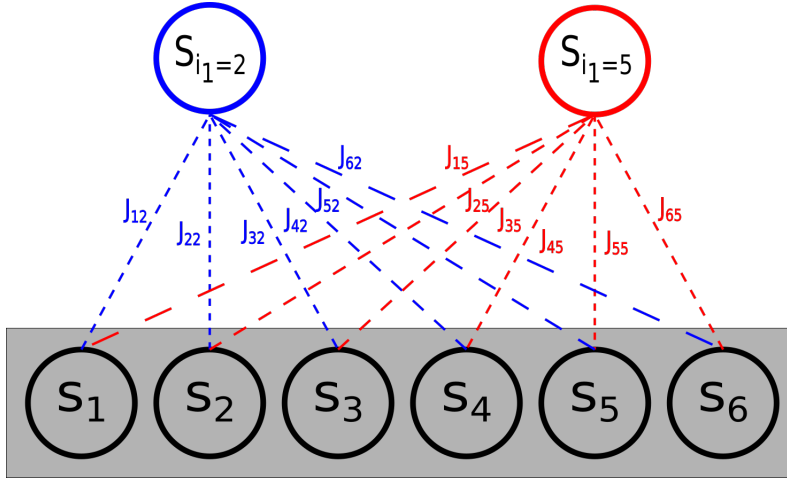


Figure 2.1.: Figure depicting the notation for the coupling strength H_1 .

As this is a many-body problem with no exact solution, a perturbative approach is taken, seeing H_1 as the perturbation of the free energy levels of H_0 . This means that the energy scales of H_1 , i.e. J_{ni_r} , need to be small against those of H_0 , i.e. t . This can be understood as a restriction for the coupling strengths, but since *small* is rather arbitrary, it is not obvious for which energy scales the theory becomes inapplicable, requiring decisions on a case-by-case basis.

Following Ref. [46], the first order (linear-in- J) variation of H_0 's energy levels are given by the effective Hamiltonian

$$H^{\text{eff}} = P_0 H_1 P_0 . \quad (2.1.2)$$

P_0 is the projector onto the Γ -fold degenerate N -electron ground state of H_0 , i.e. $P_0 = \sum_{\gamma=1}^{\Gamma} |FS, \gamma\rangle\langle FS, \gamma|$. The state is obtained by occupying all one-particle levels below or equal to the Fermi energy, $\varepsilon_k \leq \varepsilon_F$, whereby the filled states with $\varepsilon_k < \varepsilon_F$ are called the Fermi sea $|FS\rangle$. The numerical calculations in this thesis will only treat the case of incompletely occupied one-particle orbitals with energy ε_F , i.e. $\Gamma > 1$. In Ref. [32] this is referred to as the "on-resonance case". As $\Gamma = 1$ stands for a fully occupied Fermi energy level, which is a state in which there is no coupling between conduction electrons and impurities, since the former are bound in singlets due to the Pauli exclusion principle, it will not be discussed in this thesis any further.

Using Eq. (2.1.1) and the fact that P_0 only acts on the conduction electron space and is independent of the index n , one gets

$$H^{\text{eff}} = \sum_{r=1}^R \sum_{\alpha}^{\{x,y,z\}} \sum_{n=1}^L J_{ni_r}^{(\alpha)} (P_0 s_n^{(\alpha)} P_0) S_{i_r}^{(\alpha)}. \quad (2.1.3)$$

It proves useful to analyse this effective Hamiltonian in momentum space. The hopping matrix $t_{jj'}$ is per requirement diagonalizable using a unitary transformation matrix U . Transforming the operators appearing in H_0 using U gives

$$c_{j\sigma} = \sum_{k,g} U_{j,k,g} c_{k,g,\sigma}, \quad (2.1.4)$$

whereby k is the wave number and $g = 1, \dots, G(k)$ the degeneracy of the $|k, g, \sigma\rangle$ orbital. The fact that the indices k, g correspond to the wave number and thus to the energy of the orbitals, follows directly from the diagonalization of $t_{jj'}$, with its eigenvalues $\varepsilon(k)$ being the eigenenergies of the unperturbed system,

$$H_0 = \sum_{kg\sigma} \varepsilon(k) c_{kg,\sigma}^\dagger c_{kg,\sigma}. \quad (2.1.5)$$

Thus, the transformation matrix of $t_{jj'}$ executes the transformation from real space to momentum space. Applying it to the spin operator $\mathbf{s}_n = \frac{1}{2} \sum_{\sigma\sigma'} c_{n\sigma}^\dagger \boldsymbol{\sigma}_{\sigma\sigma'} c_{n\sigma'}$, leads to

$$\mathbf{s}_n = \frac{1}{2} \sum_{kk', gg', \sigma\sigma'} U_{kg;n}^\dagger c_{kg,\sigma}^\dagger \boldsymbol{\sigma}_{\sigma\sigma'} c_{k'g',\sigma'} U_{n;k'g'}. \quad (2.1.6)$$

Inserting this into Eq. (2.1.3), one has to examine the term $P_0 \mathbf{s}_n P_0$. The projector P_0 always projects onto a filled Fermi sea (FS), as the degeneracy of the ground state is only

2. Non-local, anisotropic coupling of multiple impurities to a finite lattice

dependent on the Fermi energy level. It is thus apparent that if an electron with $k' < k_F$ is annihilated by $c_{k'g'\sigma'}$, it needs to be re-created by $c_{kg\sigma}^\dagger$ with the same quantum numbers, otherwise the scalar product of $\langle FS | c_{kg\sigma}^\dagger c_{k'g'\sigma'} | FS \rangle$ returns 0. Thus, for $k, k' < k_F$ one gets $\langle FS | c_{kg\sigma}^\dagger c_{k'g'\sigma'} | FS \rangle = \delta_{kk'} \delta_{gg'} \delta_{\sigma\sigma'}$, and using the unitary properties of U , $P_0 \mathbf{s}_n P_0$ becomes

$$P_0 \mathbf{s}_n P_0 = \frac{1}{2} \sum_{\sigma} \boldsymbol{\sigma}_{\sigma\sigma} + \frac{1}{2} \sum_{gg', \sigma\sigma'} U_{k_F g; n}^\dagger c_{k_F g \sigma}^\dagger \boldsymbol{\sigma}_{\sigma\sigma'} c_{k_F g' \sigma'} U_{n; k_F g'} P_0. \quad (2.1.7)$$

The first term vanishes since the Pauli matrices are traceless, concluding in

$$P_0 \mathbf{s}_n P_0 = \frac{1}{2} \sum_{gg', \sigma\sigma'} U_{k_F g; n}^\dagger c_{k_F g \sigma}^\dagger \boldsymbol{\sigma}_{\sigma\sigma'} c_{k_F g' \sigma'} U_{n; k_F g'} P_0. \quad (2.1.8)$$

Inserting the result above into Eq. (2.1.3) returns the effective Hamiltonian:

$$H^{\text{eff}} = \sum_{r=1}^R \sum_{\alpha}^{\{x,y,z\}} \sum_{gg', \sigma\sigma'} \frac{1}{2} c_{k_F g \sigma}^\dagger \boldsymbol{\sigma}_{\sigma\sigma'}^{(\alpha)} c_{k_F g' \sigma'} \sum_{n=1}^L \left[J_{ni_r}^{(\alpha)} U_{k_F g; n}^\dagger U_{n; k_F g'} \right] S_{i_r}^{(\alpha)} P_0. \quad (2.1.9)$$

The term $\sum_{\alpha} \sum_{\sigma\sigma'} \frac{1}{2} c_{k_F g \sigma}^\dagger \boldsymbol{\sigma}_{\sigma\sigma'}^{(\alpha)} c_{k_F g' \sigma'}$ bears similarities to a spin, and differs only in the degeneracy indices g, g' , that are not necessarily equal for the creation and annihilation operators. It is desirable to transform Eq. (2.1.9) in such a way, that one obtains a spin operator, as it would then correspond to an impurity spin coupling to conduction electron spin densities, defined in momentum space, with $k = k_F$. Since usually $G(k_F) \ll L$, this would be equivalent to a decrease of relevant conduction electron spin densities compared to the many-body problem defined by the Hamiltonian (2.1.1). The aim of the following calculation is therefore to obtain a Kronecker delta from the term

$$\sum_{n=1}^L J_{ni_r}^{(\alpha)} U_{k_F g; n}^\dagger U_{n; k_F g'}. \quad (2.1.10)$$

This has the form of a dyadic product, with the n th row of U (called U_n) being multiplied with the n th column of U^\dagger (called U_n^\dagger). Defining Eq. (2.1.10) as the element of a matrix

$$\underline{M}(\alpha, r)_{gg'} := \sum_{n=1}^L J_{ni_r}^{(\alpha)} U_{k_F g; n}^\dagger U_{n; k_F g'}, \quad (2.1.11)$$

one obtains

$$\underline{M}(\alpha, r) := \sum_{n=1}^L J_{ni_r}^{(\alpha)} U_n^\dagger U_n, \quad (2.1.12)$$

in which the dependencies α and r for \underline{M} are left out from now on, as they are implied in $J_{ni_r}^{(\alpha)}$. This is a linear combination of dyadic products. To obtain the desired spin densities in Eq. (2.1.9), \underline{M} has to be diagonalized. It shall be emphasized at this point, that Eq. (2.1.12) does not correspond to a dyadic product sum of row and column vectors of unitary operators (which would be pairwise orthogonal), as the sum does not cover all the indices, but rather only the degrees of degeneracy for the Fermi energy k_F . In general, it thus forms a sum of dyadic products of non-orthogonal vectors.

The product $U_n^\dagger U_n$ is a $G(k_F) \times G(k_F)$ matrix, with thus $G(k_F)$ eigenvalues. Naming the complete $G(k_F)$ -dimensional Hilbert-Space \mathcal{H} , one finds the subset

$$\mathcal{H}_1 \equiv \text{span}\{U_1, U_2, \dots, U_L\} \subseteq \mathcal{H}. \quad (2.1.13)$$

As the vectors U_n are generally non-orthogonal, this is not necessarily a basis. Per definition the matrix \underline{M} is an endomorphism defined in $\underline{M} : \mathcal{H} \rightarrow \mathcal{H}$. Defining $\overline{\mathcal{H}}_1$ as the complement of \mathcal{H}_1 , i.e. $\mathcal{H} = \mathcal{H}_1 + \overline{\mathcal{H}}_1$, it is apparent from the definitions (2.1.12) and (2.1.13), that $\underline{M} : \mathcal{H} = \mathcal{H}_1 + \overline{\mathcal{H}}_1 \rightarrow \mathcal{H}_1$. This implies that, without loss of generality, \underline{M} is redefinable as an endomorphism in \mathcal{H}_1

$$\underline{M}|_{\mathcal{H}_1} =: \underline{M}' : \mathcal{H}_1 \rightarrow \mathcal{H}_1 \quad (2.1.14)$$

$$v \mapsto \underline{M}v. \quad (2.1.15)$$

This new matrix only includes the non-trivial portions of \underline{M} and is of dimension $\dim \mathcal{H}_1 \leq G(k_F)$. As the value $\dim \mathcal{H}_1$ is a central variable in this theory, it shall henceforth be referred to as $\eta := \dim \mathcal{H}_1$. This new matrix \underline{M}' has η eigenvalues, called $\lambda_1^{(\alpha)}(r), \dots, \lambda_\eta^{(\alpha)}(r)$ from here on out. These do, per definition, correspond to the eigenvalues of \underline{M} , whereby the other $G(k_F) - \eta$ eigenvalues are zero. That means, under the assumption that the coupling is real and not complex (i.e. the case where \underline{M} is hermitian), it is possible to transform \underline{M} and cast it into a diagonal matrix D , using a unitary transformation $V(r, \alpha)$

This corresponds to an effective spin model with the impurity spin \mathbf{S}_{i_r} coupling to up to η different delocalized spin orbitals $\mathbf{s}_\ell(r)$, with the effective coupling strengths $\lambda_\ell^{(\alpha)}(r)$. Therefore, η is the value that distinguishes between underscreening ($\eta < 2S_{i_r}$), complete screening ($\eta = 2S_{i_r}$) or overscreening ($\eta > 2S_{i_r}$). Care must be taken, because these definitions of the screening regimes are only valid when all the orbitals η are singly occupied. The delocalized spin orbitals can be calculated with $|F, \ell, r, \sigma, \alpha\rangle = c_{k_F \ell \sigma}^\dagger(r, \alpha)|\text{vac.}\rangle$, which is equivalent to

$$|F, \ell, r, \sigma, \alpha\rangle = \sum_g V_{g\ell}(r, \alpha) \sum_i U_{i; k_F g} |i, \sigma\rangle, \quad (2.1.25)$$

whereby $V_{g\ell}(r, \alpha)$ summed over g equals the sum over the components of the eigenvector to the eigenvalue $\lambda_\ell^{(\alpha)}(r)$, which is dependent on the lattice and coupling strengths.

This formalism also includes the local case developed in Ref. [32]. In this case the coupling strength matrix is given by isotropic local coupling, i.e.

$$J_{ni_r}^{(\alpha)} = \delta_{ni_r} J. \quad (2.1.26)$$

Thus, $\underline{M}(r) = J U_{i_r}^\dagger U_{i_r}$ and $\eta = 1$. The eigenvector is given by $U_{i_r}^\dagger$, since

$$\underline{M}(r) U_{i_r}^\dagger = (J U_{i_r}^\dagger U_{i_r}) U_{i_r}^\dagger = (J \sum_g |U_{i_r; k_F g}|^2) U_{i_r}^\dagger, \quad (2.1.27)$$

with the eigenvalue $\lambda_1(r) = J \sum_g |U_{i_r; k_F g}|^2 \equiv J_{\text{eff}}(r)$. Inserting this into Eq. (2.1.24), one gets

$$H^{\text{eff}} = \sum_{r=1}^R J_{\text{eff}}(r) \mathbf{s}_{\ell=1}(i_r) \mathbf{S}_{i_r}, \quad (2.1.28)$$

with the orbitals

$$|F, r, \sigma\rangle = \frac{1}{\sqrt{\sum_g |U_{i_r; k_F g}|^2}} \sum_{g=1}^{G(k_F)} U_{k_F g; i_r}^\dagger \sum_{i=1}^L U_{i; k_F g} |i, \sigma\rangle, \quad (2.1.29)$$

which corresponds exactly to the results found in Ref. [32].

2.2. Numerical results

This Sec. focuses on the discussion of the numerical calculation results obtained for two exemplary one-dimensional conduction electron lattices. The limitation to one dimension

2. Non-local, anisotropic coupling of multiple impurities to a finite lattice

is purely for simplicities sake. The focus of this thesis is merely to derive a formalism that adequately describes overscreening, for which one-dimensional systems will serve as a proof-of-concept, while a discussion of more general systems are out of the scope of this work. A more detailed analysis of various systems will be published later [33].

We assume the systems to follow the tight-binding regime, i.e.

$$t_{jj'} = \begin{cases} t, & \text{if } j \text{ and } j' \text{ are next-neighbours} \\ 0, & \text{else} \end{cases} \\ = t(\delta_{j,j'+1} + \delta_{j,j'-1}). \quad (2.2.1)$$

It is easily verifiable that this fulfills the restriction on the hopping matrix, i.e. that it is diagonalizable with a unitary transformation U , since it is hermitian. Furthermore, the coupling strength matrix in the α -direction $J_{ni_r}^{(\alpha)}$ is taken to be isotropic (no α dependency) and restricted to local and next-neighbour coupling:

$$J_{ni_r} = \begin{cases} J_{\text{local}}, & \text{if } n = i_r \\ J_{nn}, & \text{if } n \text{ and } i_r \text{ are next-neighbours} \\ 0, & \text{else} \end{cases} \\ = J_{\text{local}}\delta_{ni_r} + J_{nn}(\delta_{n,i_r+1} + \delta_{n,i_r-1}). \quad (2.2.2)$$

Regarding the energy scales, only J_{nn} is varied, while $t = J_{\text{local}} \equiv 1$ are constant. Concerning the discussion about the valid energy scales for the perturbative approach made in this thesis (see beginning of Sec. 2.1), the variations of J_{nn} will be out of the range of what one would normally consider *small* against t , with values as high as $|J_{nn}| = 10^4$ and discussions for the limiting case $J_{nn} \rightarrow \infty$. In fact, $J_{\text{local}} = t$ might already be out of this scope. This is justifiable as the model is linear in nature. Looking at the effective Hamiltonian (2.1.24) and the definition of \underline{M} (2.1.10), one sees that there is a linear dependency on J_{ni_r} and the hopping t . The case of $t = 10$ with $J_{nn} = 1$ is thus equivalent to $t = 1$ and $J_{nn} = 10^{-1}$ with a prefactor 10, which, to anticipate the results, is confirmed numerically. The magnitude of the hopping matrix t thus does not qualitatively change the numerical results, they only depend on the ratio J_{nn}/J_{local} .

As a final restriction on Eq. (2.1.24), only the single impurity case ($R = 1$) will be discussed, to avoid interferences from inter-impurity interactions, like the RKKY-interaction

[28–30]. Moreover, the impurity spin is modelled to be $S_{i_1} = 1/2$. This means that the criterion for overscreening $\eta > 2S_{i_r}$ [34] becomes $\eta > 1$ (with all η orbitals singly occupied). There are two possible boundary conditions for one-dimensional lattices, open boundary conditions (i.e. chains with loose ends) and periodic boundary conditions (i.e. rings). In the former case one obtains $\eta \equiv 1$, because the eigenvalues of $t_{jj'}$ are non-degenerate for open boundary conditions [47]. As this precludes overscreening, it will not be discussed any further at this point (see Sec. 3.2 for one-dimensional systems with open boundary conditions). Fig. 2.2(a) illustrates the kind of ring lattices that were evaluated in the numerical calculations, only that the lattice length was $L = 100$ and $i_1 = 10$. This system is completely symmetric to any translation of the impurity to other sites, as there is ring symmetry. Thus, the choice of $i_1 = 10$ is arbitrary and of no further relevance. $L = 100$ directly influences the energy levels, but has no impact on the qualitative results. The energy levels for such one-dimensional rings are derived in App. A and illustrated in Fig. 2.2(b).

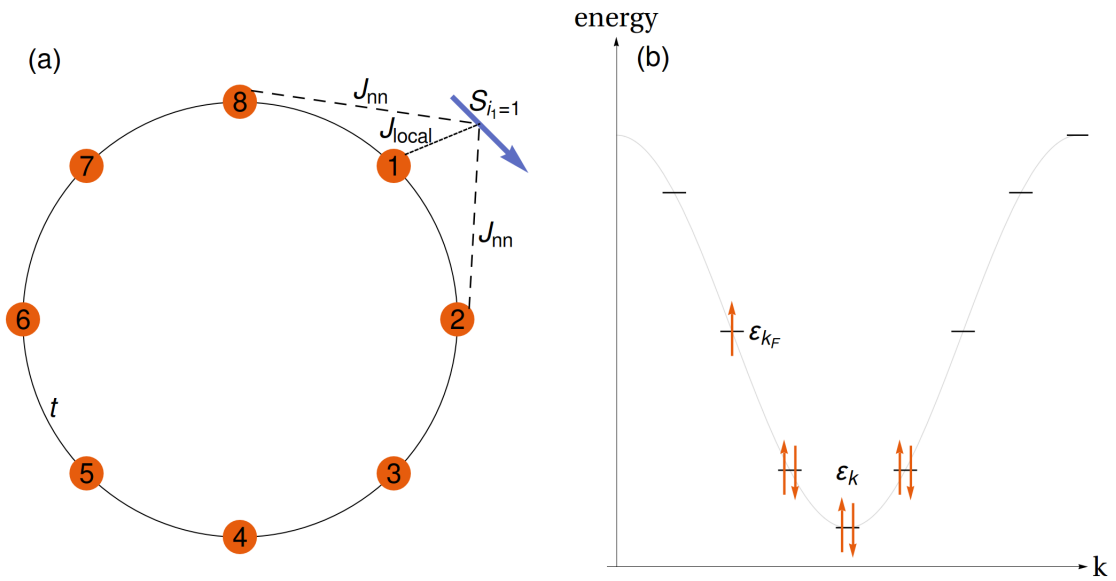


Figure 2.2.: (a) Illustration of a lattice with $L = 8$ sites and hopping t . A single impurity spin, sitting at $i_1 = 1$, is coupling, with local and next-neighbour coupling, to the lattice. (b) Corresponding energy diagram with $N = 7$ conduction electrons in the ground state. This case corresponds to $G(k_F) = 2$, $\Gamma = 4$ and one k_F -electron.

2. Non-local, anisotropic coupling of multiple impurities to a finite lattice

The number of delocalized orbitals η for one-dimensional rings is

$$\eta = \begin{cases} 2, & J_{nn} \neq 0 \\ 1, & J_{nn} = 0 \end{cases}.$$

The effective Hamiltonian (2.1.24) thus becomes

$$H^{\text{eff}} = \sum_{\ell=1}^2 \lambda_{\ell} \mathbf{s}_{\ell} \mathbf{S} P_0 \quad (2.2.3)$$

in the $J_{nn} \neq 0$ case. This corresponds to an impurity spin coupling to two delocalized orbitals in the metal, or a central spin model with three spins. This is illustrated in Fig. 2.3(a) with its effective coupling constants λ_1, λ_2 plotted in Fig. 2.3(b). While

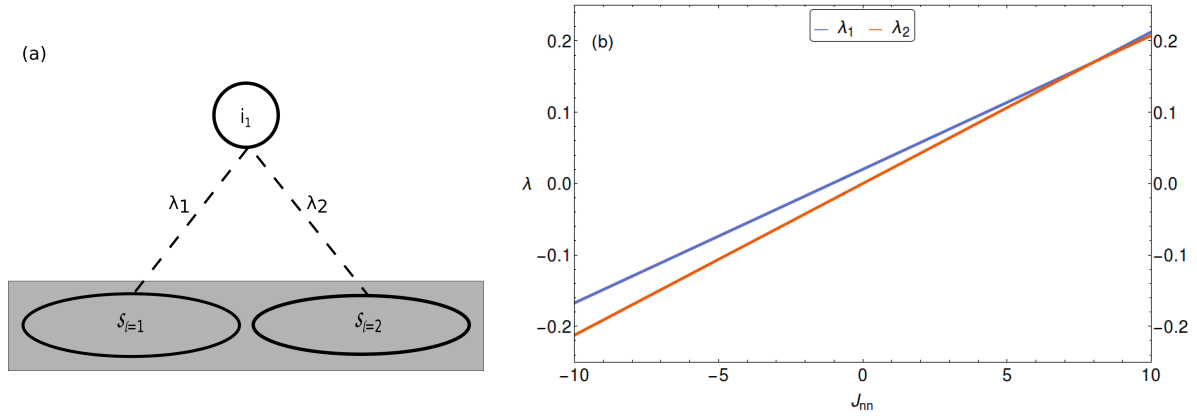


Figure 2.3.: (a) Illustration of the general orbital scheme in one-dimensional systems with open boundary conditions and one impurity spin. (b) Corresponding plot of effective coupling constants λ_1 (λ_2) in blue (red) in arb. units against J_{nn} .

$\lambda_1 > \lambda_2$ for J_{nn} around 0 with differences of order $J_{nn}/10$, they approach each other for increasing coupling strengths, with the smallest distance at around $J_{nn} = 7.5$. For $J_{nn} \rightarrow \pm\infty$ they diverge from each other again with a constant relative difference of around $|\lambda_1 - \lambda_2| = J_{nn}/100$. This is surprising because the $J_{nn} \rightarrow \pm\infty$ limiting case is equivalent to $J_{\text{local}} \rightarrow 0$, i.e. the case of an impurity that only couples to the next neighbours in real space, which is a case that should be highly symmetric. The transition to the effective model thus corresponds to a mapping of symmetric coupling to two spin orbitals with J_{nn} in real space to asymmetric coupling to two delocalized spin orbitals with λ_1, λ_2 . It is not clear at which point this symmetry is broken and whether it is a shortcoming of

the perturbative approach or a numerical error.

The questions to be answered now, is how the k_F -electrons effectively couple to the impurity spin with these λ_i , i.e. what ground state the system takes. For that the analysis has to be split up according to the number of k_F -electrons. The energy levels are up to two-fold degenerate. Only the lowest and the highest energy level are not degenerate, the latter only for even lattice lengths. Thus, in the "on-resonance case" $\Gamma > 1$, there are up to three possible k_F -electrons, whereby the case for one and three k_F -electrons can be treated jointly as, in the latter case, two electrons end up in the same orbital and form a singlet due to the Pauli exclusion principle, effectively leaving one free k_F -electron. The numbers that were used for the numerical evaluations are $N = 51$ for one k_F -electron and $N = 52$ for two k_F -electrons. These two cases are discussed separately in Sec. 2.2.1 and 2.2.2 respectively.

2.2.1. One Fermi electron

With only one k_F -electron in the ground state, the effective Hamiltonian (2.2.3) describes a three-spin problem for two particles. The possible states are thus a triplet ($S_{\text{tot}} = 1$) or singlet ($S_{\text{tot}} = 0$), since the unoccupied spin state can be ignored. One does not a priori know to which of the two delocalized orbitals ℓ the impurity couples to. This can be determined through the analysis of the various quantum numbers. The quantum number S_{tot} of the total spin $\mathbf{S}_{\text{tot}} = \mathbf{S}_{\text{elec}} + \mathbf{S}_{\text{imp}} = \mathbf{s}_1 + \mathbf{s}_2 + \mathbf{S}_{\text{imp}}$ is plotted against J_{nn} in Fig. 2.4(a). It can be seen that in phase I the system forms a triplet, which indicates ferromagnetic coupling, while in phase II the system forms a singlet, which indicates anti-ferromagnetic coupling.

Fig. 2.4(b) shows the calculation results for the ground state energies, in which can be perceived, that the phase transition from ferromagnetic to anti-ferromagnetic coupling coincides with the splitting up of ground state energies for $|m_{S_{\text{tot}}}| = 1$ and $|m_{S_{\text{tot}}}| = 0$. This confirms the results from Fig. 2.4(a), because in phase I the state of the system is a triplet with $m_{S_{\text{tot}}} \in \{-1, 0, 1\}$, i.e. a state in which no distinction is made based upon the spin in z-direction. In phase II the ground state energy for $|m_{S_{\text{tot}}}| = 0$ is lower than that of $|m_{S_{\text{tot}}}| = 1$, which means that the ground state energy for a singlet (which has

2. Non-local, anisotropic coupling of multiple impurities to a finite lattice

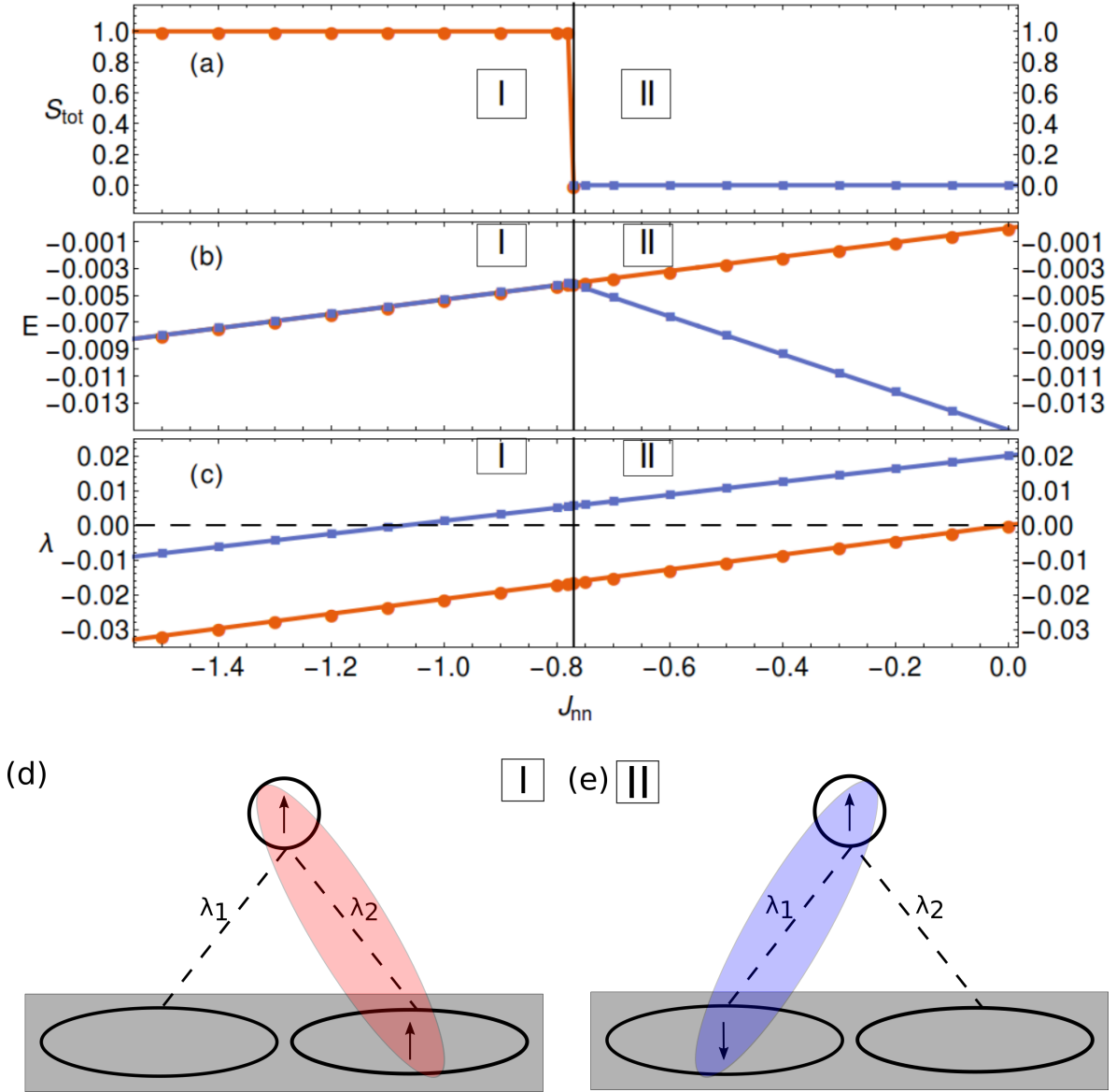


Figure 2.4.: Plots of various numerical results for a one-dimensional ring with $J_{local} = t = 1$, $L = 100$, $N = 51$ and varying next neighbour coupling strengths J_{nn} . Through (a)-(c), phase I is marked for $J_{nn} < -0.77$ and phase II is for $J_{nn} > -0.77$. (a) Plot of the quantum number S_{tot} extracted from the expectation value for the total spin $\langle \mathbf{S}_{tot}^2 \rangle$. The colour change emphasizes the change of the orbital to which the impurity couples. (b) Plot of the ground state energies in arb. units for $|m_{S_{tot}}|=0$ ($|m_{S_{tot}}|=1$) in blue (red). (c) Plot of the effective coupling constants λ_1 (λ_2) in blue (red). This is a more detailed version of Fig. 2.3(b). Schematic pictures (d) for the ferromagnetic state in phase I and (e) for the anti-ferromagnetic state in phase IIa.

$|m_{S_{\text{tot}}} \equiv 0\rangle$ is lower than for a triplet and the system thus forms a singlet in the ground state.

Lastly, the plot of effective coupling constants λ_1, λ_2 also confirms this transition. The calculation of the ground state energies as a function of the effective coupling constants, for singlets and triplets, is done in App. B. Applying the results to this system gives

$$\langle H^{\text{eff}} \rangle_{\text{triplet}}^{(\ell)} = \frac{\lambda_\ell}{4}, \quad (2.2.4)$$

$$\langle H^{\text{eff}} \rangle_{\text{singlet}}^{(\ell)} = -\frac{3\lambda_\ell}{4}. \quad (2.2.5)$$

Negative effective coupling constants thus favour ferromagnetic coupling and positive ones favour anti-ferromagnetic coupling. Looking at the coupling constants of the system at hand, one finds $\langle H^{\text{eff}} \rangle_{\text{triplet}}^{(2)} < \langle H^{\text{eff}} \rangle_{\text{singlet}}^{(1)}$ in phase I. Thus the system forms a triplet with the electron in the second orbital, which is depicted in Fig. 2.4(d). The transition to phase II marks the point at which $\langle H^{\text{eff}} \rangle_{\text{singlet}}^{(1)}$ becomes smaller than $\langle H^{\text{eff}} \rangle_{\text{triplet}}^{(2)}$. Because it is energetically more favourable, the system forms a singlet with the first orbital, which is depicted in Fig. 2.4(e).

In conclusion, one finds that the impurity is screened by the only k_F -electron for large enough coupling strengths. This corresponds to complete screening, which is expected in the normal single channel Kondo effect.

2.2.2. Two Fermi electrons

For the evaluation of the results for two k_F -electrons it is helpful to develop the basis of possible states that can arise in this problem. There are two k_F -electron spins and one impurity spin. The effective Hamiltonian (2.2.3) thus essentially becomes a central spin problem with three spin states occupied by three particles. Using the following basis, naming the z-component of the impurity spin IMP and the z-component of the ℓ th orbital spin OS_ℓ ,

$$\begin{aligned} |\text{IMP}, \text{OS}_1, \text{OS}_2\rangle \in \text{span}\{ & |1\rangle = |\uparrow, \uparrow, \uparrow\rangle, |2\rangle = |\downarrow, \uparrow, \uparrow\rangle, |3\rangle = |\uparrow, \downarrow, \uparrow\rangle, \\ & |4\rangle = |\uparrow, \uparrow, \downarrow\rangle, |5\rangle = |\downarrow, \downarrow, \uparrow\rangle, |6\rangle = |\downarrow, \uparrow, \downarrow\rangle, \\ & |7\rangle = |\uparrow, \downarrow, \downarrow\rangle, |8\rangle = |\downarrow, \downarrow, \downarrow\rangle\}, \end{aligned}$$

2. Non-local, anisotropic coupling of multiple impurities to a finite lattice

the matrix form of H^{eff} from Eq. (2.2.3) becomes

$$H^{\text{eff}} = \begin{pmatrix} \frac{\lambda_1 + \lambda_2}{4} & 0 & 0 & 0 & 0 & 0 & 0 & 0 \\ 0 & -\frac{\lambda_1 + \lambda_2}{4} & \frac{\lambda_1}{2} & \frac{\lambda_2}{2} & 0 & 0 & 0 & 0 \\ 0 & \frac{\lambda_1}{2} & \frac{\lambda_2 - \lambda_1}{4} & 0 & 0 & 0 & 0 & 0 \\ 0 & \frac{\lambda_2}{2} & 0 & \frac{\lambda_1 - \lambda_2}{4} & 0 & 0 & 0 & 0 \\ 0 & 0 & 0 & 0 & \frac{\lambda_1 - \lambda_2}{4} & 0 & \frac{\lambda_2}{2} & 0 \\ 0 & 0 & 0 & 0 & 0 & \frac{\lambda_2 - \lambda_1}{4} & \frac{\lambda_1}{2} & 0 \\ 0 & 0 & 0 & 0 & \frac{\lambda_2}{2} & \frac{\lambda_1}{2} & -\frac{\lambda_1 + \lambda_2}{4} & 0 \\ 0 & 0 & 0 & 0 & 0 & 0 & 0 & \frac{\lambda_1 + \lambda_2}{4} \end{pmatrix}. \quad (2.2.6)$$

The energy states the system can take, i.e. the eigenvalues of H^{eff} , are given by the roots of the characteristic polynomial

$$\begin{aligned} 0 &= \det(H^{\text{eff}} - \mathbf{1}\varepsilon) \\ &= \left(\frac{\lambda_1 + \lambda_2}{4} - \varepsilon \right)^4 \left(\frac{3}{16}(\lambda_1 - \lambda_2)^2 - \frac{\lambda_1 + \lambda_2}{2}\varepsilon - \varepsilon^2 \right)^2, \end{aligned}$$

which are

$$\varepsilon_0 = \frac{\lambda_1 + \lambda_2}{4}, \quad \varepsilon_{1,2} = \frac{1}{4} \left(-(\lambda_1 + \lambda_2) \pm 2\sqrt{\lambda_1^2 - \lambda_1\lambda_2 + \lambda_2^2} \right). \quad (2.2.7)$$

To determine the actual spin state of the system one needs to find the corresponding eigenvectors to these eigenvalues.

These are defined by the following system of linear equations (with a degeneracy index i)

$$H^{\text{eff}}|\varepsilon_j, i\rangle = \varepsilon_j|\varepsilon_j, i\rangle \quad j \in \{0, 1, 2\},$$

to which the solution for the first eigenenergy can be found as

$$\begin{aligned} |\varepsilon_0, 1\rangle &= |1\rangle, \\ |\varepsilon_0, 2\rangle &= \frac{1}{\sqrt{3}}(|2\rangle + |3\rangle + |4\rangle), \\ |\varepsilon_0, 3\rangle &= \frac{1}{\sqrt{3}}(|5\rangle + |6\rangle + |7\rangle), \\ |\varepsilon_0, 4\rangle &= |8\rangle. \end{aligned}$$

For the second and third eigenenergies,

$$\begin{aligned}
 |\varepsilon_{1/2}, 1\rangle &= \frac{1}{\sqrt{c(\varepsilon_{1/2})}} \left(|2\rangle + \left(\frac{\lambda_1}{-\lambda_2 \pm \sqrt{\lambda_1 - \lambda_1\lambda_2 + \lambda_2}} \right) |3\rangle \right. \\
 &\quad \left. + \left(\frac{\lambda_2}{-\lambda_1 \pm \sqrt{\lambda_1^2 - \lambda_1\lambda_2 + \lambda_2^2}} \right) |4\rangle \right), \tag{2.2.8}
 \end{aligned}$$

$$\begin{aligned}
 |\varepsilon_{1/2}, 2\rangle &= \frac{1}{\sqrt{c(\varepsilon_{1/2})}} \left(\left(\frac{\lambda_2}{-\lambda_1 \pm \sqrt{\lambda_1^2 - \lambda_1\lambda_2 + \lambda_2^2}} \right) |5\rangle \right. \\
 &\quad \left. + \left(\frac{\lambda_1}{-\lambda_2 \pm \sqrt{\lambda_1 - \lambda_1\lambda_2 + \lambda_2}} \right) |6\rangle + |7\rangle \right), \tag{2.2.9}
 \end{aligned}$$

whereby $c(\varepsilon_{1/2})$ are the normalization parameters:

$$c(\varepsilon_{1/2}) = 1 + \left(\frac{\lambda_1}{-\lambda_2 \pm \sqrt{\lambda_1 - \lambda_1\lambda_2 + \lambda_2}} \right)^2 + \left(\frac{\lambda_2}{-\lambda_1 \pm \sqrt{\lambda_1^2 - \lambda_1\lambda_2 + \lambda_2^2}} \right)^2.$$

Using these eigenvectors one can easily identify the expectation values of the spin operators. The spin operator for the conduction electrons, defined as the sum of the two orbital spins, can be written as

$$\begin{aligned}
 \mathbf{S}_{\text{elec}}^2 &:= (\mathbf{s}_1 + \mathbf{s}_2)^2, \\
 &= s_1^2 + s_2^2 + 2\mathbf{s}_1\mathbf{s}_2, \\
 &= s_1^2 + s_2^2 + s_1^+ s_2^- + s_1^- s_2^+ + 2s_1^z s_2^z, \tag{2.2.10}
 \end{aligned}$$

with the ladder operators $s^\pm := s^x \pm is^y$.

Analogously, one finds for the total spin

$$\begin{aligned}
 \mathbf{S}_{\text{tot}}^2 &= (\mathbf{S}_{\text{elec}} + \mathbf{S}_{\text{imp}})^2, \\
 &= S_{\text{elec}}^2 + S_{\text{imp}}^2 + 2\mathbf{S}_{\text{elec}}\mathbf{S}_{\text{imp}}, \\
 &= S_{\text{elec}}^2 + S_{\text{imp}}^2 + s_1^+ S_{\text{imp}}^- + s_1^- S_{\text{imp}}^+ + s_2^+ S_{\text{imp}}^- + s_2^- S_{\text{imp}}^+ \\
 &\quad + 2s_1^z S_{\text{imp}}^z + 2s_2^z S_{\text{imp}}^z. \tag{2.2.11}
 \end{aligned}$$

The expectation values in the state ε_0 are constant:

$$\begin{aligned}
 \langle \varepsilon_0, i | \mathbf{S}_{\text{elec}}^2 | \varepsilon_0, i \rangle = 2 &\quad \Rightarrow \quad S_{\text{elec}} = 1 \quad \forall i \in \{1, 2, 3, 4\}, \\
 \langle \varepsilon_0, i | \mathbf{S}_{\text{tot}}^2 | \varepsilon_0, i \rangle = \frac{15}{4} &\quad \Rightarrow \quad S_{\text{tot}} = \frac{3}{2} \quad \forall i \in \{1, 2, 3, 4\}.
 \end{aligned}$$

2. Non-local, anisotropic coupling of multiple impurities to a finite lattice

For $\varepsilon_{1/2}$ one finds only one constant:

$$\langle \varepsilon_{1/2}, i | \mathbf{S}_{\text{tot}}^2 | \varepsilon_{1/2}, i \rangle = \frac{3}{4} \quad \Rightarrow \quad S_{\text{tot}} = \frac{1}{2} \quad \forall i \in \{1, 2\}. \quad (2.2.12)$$

The expectation value for $\langle \varepsilon_{1/2}, i | S_{\text{elec}}^2 | \varepsilon_{1/2}, i \rangle$ is a function of the two coupling constants, but independent of i (i.e. two-fold degeneracy in i), which will not be written down here, as its specific form is not of any further relevance.

Thereby the states the system can take are completely described. The numerical results that were obtained are depicted in Fig. 2.5, and the goal of the following discussion is to explain these using the just derived states.

In Fig. 2.5(a) one sees that in phase I the ground state energy corresponds exactly to ε_0 for any $|m_{S_{\text{tot}}}|$. Thus, the system's ground state is a four-fold degenerate quadruplet state. This is confirmed by looking at Fig. 2.5(b) in which one sees that in phase I $S_{\text{elec}} \equiv 1$ which corresponds to the quantum number of the electronic spin component of the state $|\varepsilon_0, i\rangle$ (i.e. parallel spins). The system is thus in a pure $|\varepsilon_0, i\rangle$ state, which is depicted in 2.6(a), with four-fold degeneracy.

In phases IIa and IIb the calculated ground state energies split up in $|m_{S_{\text{tot}}}|$ and correspond exactly to the eigenenergies ε_0 for $|m_{S_{\text{tot}}}| = 1.5$ and ε_2 for $|m_{S_{\text{tot}}}| = 0.5$, whereby the latter is the lower one. The state with $|m_{S_{\text{tot}}}| = 1.5$ will be ignored from now on, as it is a subset of eigenvectors to the eigenenergy ε_0 and not the ground state energy. It shall be noted here that the phases IIa and IIb are not different phases, as the state of the system does not change. The distinction is made for interpretation purposes that will become apparent later (see Eq. (2.2.15) and (2.2.16)).

As a confirmation for the energy diagram one sees in Fig. 2.5(b), that the expectation value $S_{\text{elec}}(|m_{S_{\text{tot}}}| = 0.5)$ in phases IIa and IIb equals exactly that of $|\varepsilon_2, i\rangle$. From that, one can gather, that the system is in the state $|\varepsilon_2, i\rangle$ with a two-fold degeneracy in i , and the question arises what the state signifies, because while the analysis of the system is technically done, the Kondo model expects singlets to be formed. As such it would be helpful to rewrite the states $|\varepsilon_2, i\rangle$ in a way that they are interpretable as singlets. One can write $|\varepsilon_2, 1\rangle$ from Eq. (2.2.8), with the original definition of the basis and a redefinition

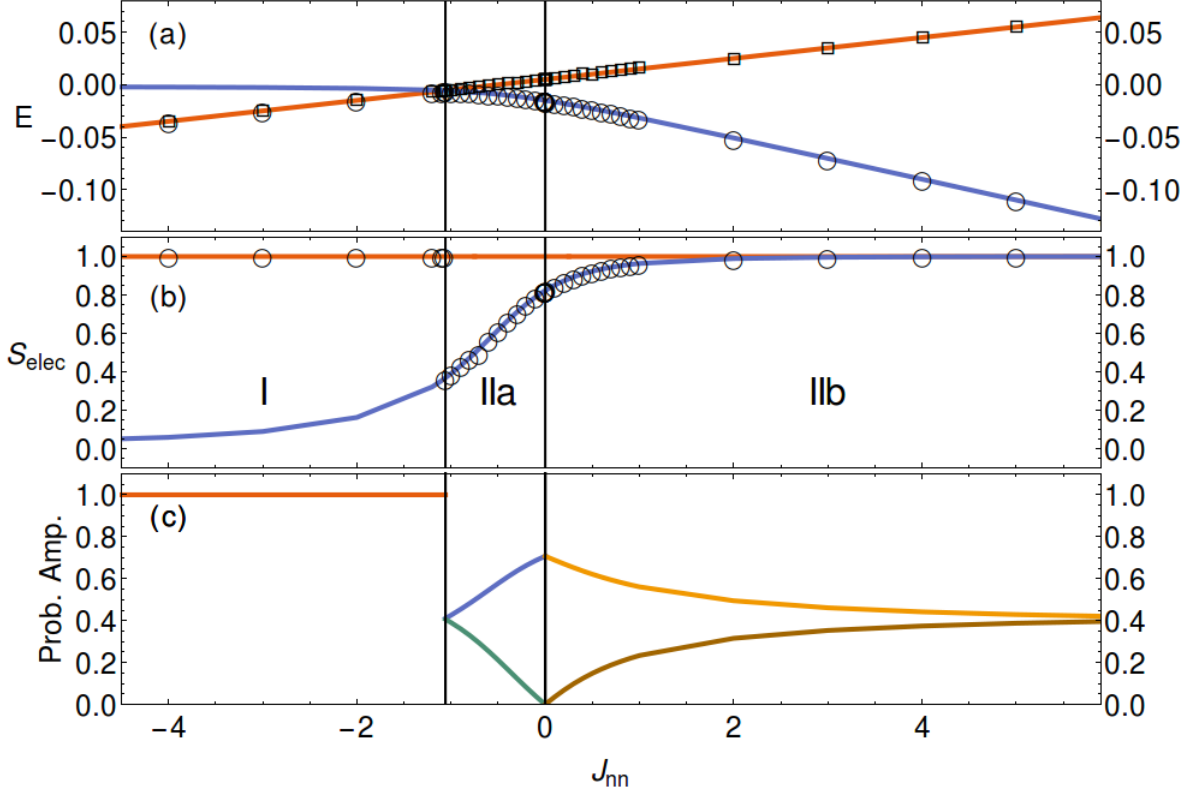


Figure 2.5.: Plots of various numerical results for a one-dimensional ring with $J_{\text{local}} = t = 1$, $L = 100$, $N = 52$ and varying next neighbour coupling strengths J_{nn} . Through (a)-(c), phase I is marked for $J_{nn} < -1.06$, phase IIa for $-1.06 \leq J_{nn} < 0$ and phase IIb for $0 \leq J_{nn}$. (a) Plots of the ground state energies (arb. units). Numerical results for $|m_{S_{\text{tot}}}| = 0.5$ (1.5) are marked in circles (squares). Underlaid are the plots of the eigenenergy ε_2 (ε_0) in blue (red). (b) Plot of the electronic spin quantum number S_{elec} . Numerical results for $|m_{S_{\text{tot}}}| = 0.5$ are marked in circles. Underlaid are the plots of the quantum numbers S_{elec} to the expectation values $\langle \varepsilon_2, i | \mathbf{S}_{\text{elec}}^2 | \varepsilon_2, i \rangle$ in blue and to $\langle \varepsilon_0, i | \mathbf{S}_{\text{elec}}^2 | \varepsilon_0, i \rangle$ in red. (c) Plot of the probability amplitudes of the composing vectors of the states in the three different phases. In phase I is the probability amplitude to have an eigenvector of ε_0 , in phase IIa $\alpha(\lambda_1, \lambda_2)$ in blue and $\beta(\lambda_1, \lambda_2)$ in green and in phase IIb $-\beta(\lambda_1, \lambda_2)$ in brown and $-\gamma(\lambda_1, \lambda_2)$ in yellow.

of the coefficients, as

$$\begin{aligned}
 |\varepsilon_2, 1\rangle &= \frac{1}{\sqrt{c(\varepsilon_2)}} \left(|2\rangle + \left(\frac{\lambda_1}{-\lambda_2 \pm \sqrt{\lambda_1 - \lambda_1 \lambda_2 + \lambda_2}} \right) |3\rangle \right. \\
 &\quad \left. + \left(\frac{\lambda_2}{-\lambda_1 \pm \sqrt{\lambda_1^2 - \lambda_1 \lambda_2 + \lambda_2^2}} \right) |4\rangle \right), \\
 &= \alpha(\lambda_1, \lambda_2) |\downarrow, \uparrow, \uparrow\rangle + \beta(\lambda_1, \lambda_2) |\uparrow, \downarrow, \uparrow\rangle + \gamma(\lambda_1, \lambda_2) |\uparrow, \uparrow, \downarrow\rangle.
 \end{aligned} \tag{2.2.13}$$

2. Non-local, anisotropic coupling of multiple impurities to a finite lattice

While this is the correct state for the system in phases IIa and IIb, it does not lend itself to interpretation. The goal is thus to rewrite this term as a combination of singlets. By adding the coefficients together, one finds that

$$\alpha(\lambda_1, \lambda_2) + \beta(\lambda_1, \lambda_2) + \gamma(\lambda_1, \lambda_2) \equiv 0. \quad (2.2.14)$$

Adding $0 = \alpha - \alpha = \beta - \beta = \gamma - \gamma$, one can now gather the two variations of Eq. (2.2.13), with which one can describe the states in phases IIa and IIb, respectively:

$$|\varepsilon_2, 1\rangle^{\text{IIa}} = \alpha(\lambda_1, \lambda_2) \underbrace{(|\downarrow, \uparrow, \uparrow\rangle - |\uparrow, \uparrow, \downarrow\rangle)}_{\text{Singlet: } IMP \text{ and } OS_2} + \beta(\lambda_1, \lambda_2) \underbrace{(|\uparrow, \downarrow, \uparrow\rangle - |\uparrow, \uparrow, \downarrow\rangle)}_{\text{Singlet: } OS_1 \text{ and } OS_2}, \quad (2.2.15)$$

$$|\varepsilon_2, 1\rangle^{\text{IIb}} = -\beta(\lambda_1, \lambda_2) \underbrace{(|\downarrow, \uparrow, \uparrow\rangle - |\uparrow, \downarrow, \uparrow\rangle)}_{\text{Singlet: } IMP \text{ and } OS_1} - \gamma(\lambda_1, \lambda_2) \underbrace{(|\downarrow, \uparrow, \uparrow\rangle + |\uparrow, \uparrow, \downarrow\rangle)}_{\text{Singlet: } IMP \text{ and } OS_2}. \quad (2.2.16)$$

These states are chosen in such a way, that the coefficients are positive in their respective phases. This also defines the transition from phase IIa to phase IIb, because even though there is no change in the state itself, the coefficient $\beta(\lambda_1, \lambda_2)$ becomes negative (see Fig. 2.5(c)), so rather than describing the state of the system with $|\varepsilon_2, 1\rangle^{\text{II}}$ in phase IIb, it proves convenient to describe it with $|\varepsilon_2, 1\rangle^{\text{IIb}}$, to avoid a mix of positive and negative coefficients, which lends itself more to interpretation. From Eqs. (2.2.15) and (2.2.16) one can see, that both phases describe singlets with one unbound spin-up particle. An analogous analysis done on $|\varepsilon_2, 2\rangle$ yields the same states with an unbound spin-down particle. Thus, there is a two-fold degeneracy in phases IIa and IIb given by the free uncoupled spin, though one should emphasize that the spin is not exactly free as there is always an entanglement of singlets, binding all three spins.

While this state is clear, analysing the progression of the singlet mixture with J_{nn} is instrumental to get a better understanding of what is happening. Looking at Fig. 2.5(c), one sees that, at the phase transition from region I to IIa, there is an entangled state, with equal probability amplitudes for the singlet between impurity spin and the second orbital spin ($\alpha(\lambda_1, \lambda_2)$) and a singlet between the two orbital spins ($\beta(\lambda_1, \lambda_2)$). As J_{nn} increases, the latter case gets suppressed up to the point of only local coupling ($J_{nn} = 0$), at which only the singlet between impurity and second conduction electron remains. This is in agreement with the fact that $\eta(J_{nn} = 0) = 1$. In phase IIb one observes, that additionally to this singlet ($-\gamma(\lambda_1, \lambda_2)$), there is another singlet between the impurity spin and the

first orbital spin $(-\beta(\lambda_1, \lambda_2))$ whose probability amplitude increases with J_{nn} . In the limit of $J_{nn} \rightarrow \infty$, one has $|\lambda_1 - \lambda_2| = 10^{-2} J_{nn}$ and thus a constant but not complete level of uncertainty about which delocalized orbital forms the singlet. These resulting states are depicted in Fig. 2.6(b) and (c).

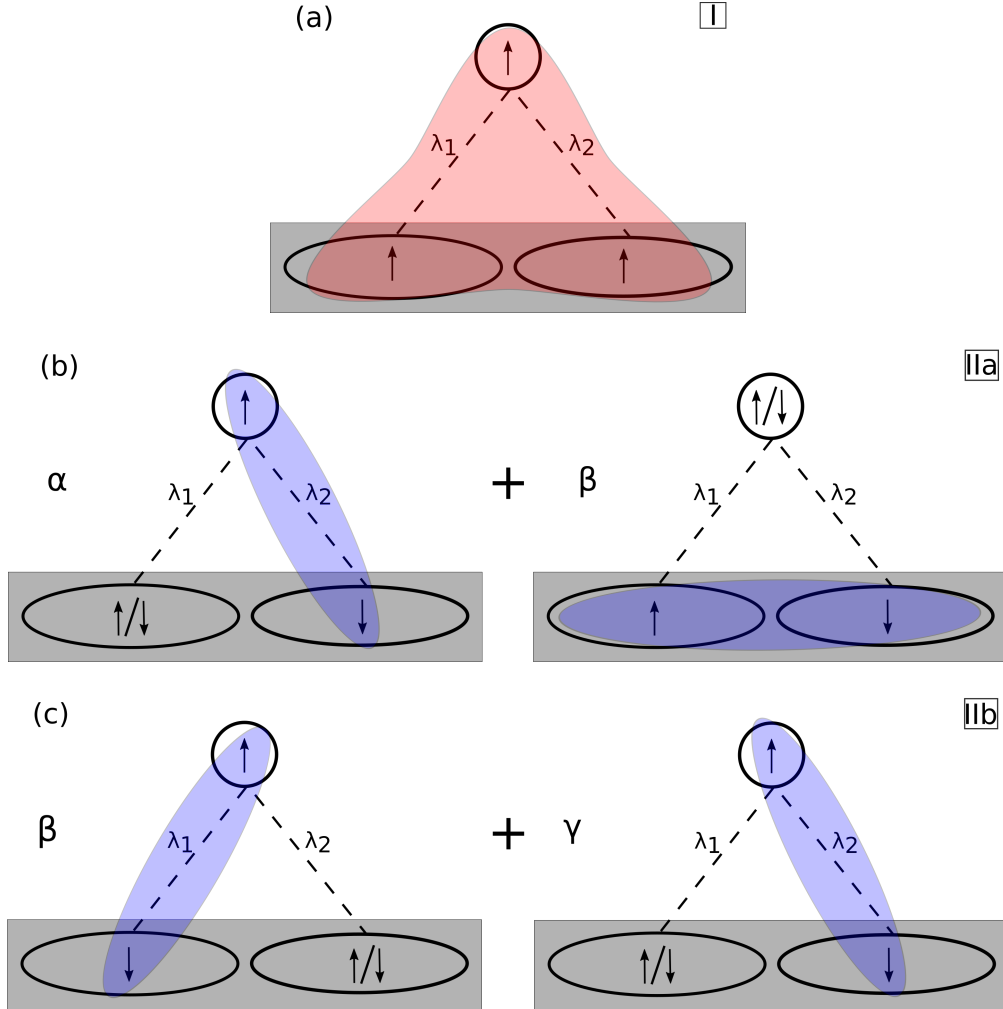


Figure 2.6.: Plot of the various states the system takes throughout the variation of J_{nn} according to the discussion in this Sec.. The complementary states to make singlets are implied. (a) State $|\varepsilon_0, 1\rangle$ as a representative for the state in phase I. Ferromagnetic quadruplet between the two conduction electrons and the impurity. (b) State $|\varepsilon_2, i\rangle^{\text{IIa}}$ in phase IIa. (c) State $|\varepsilon_2, i\rangle^{\text{IIb}}$ in phase IIb.

To conclude, the system's ground state is two-fold degenerate as soon as anti-ferromagnetic coupling begins, i.e. in phases IIa and IIb, as opposed to the case in Sec. 2.2.1 in which there was no degeneracy. Also, while $S_{\text{tot}} \equiv 0.5$, the impurity is not completely screened

2. *Non-local, anisotropic coupling of multiple impurities to a finite lattice*

in phase IIa, since there is a probability of having a conduction electron singlet, which decreases with increasing coupling strengths J_{nn} . Phase IIb is the overscreening regime, as the impurity is getting screened by one of the conduction electrons while the other one is free in an entangled singlet state, resulting in two-fold degeneracy and a number of screening channels greater than the number of impurities, thus fulfilling Nozières criteria for overscreening [34, 37]. It is apparent though, that the aforementioned difference of the effective coupling strengths λ_i leads to asymmetric coupling to both orbitals. So this cannot be considered perfectly delocalized overscreening.

3. Forced overscreening

To measure and discuss the effect of overscreening, impurities coupling to only one lattice are neither practical nor intuitive, as even the simplest case of one-dimensional lattices with local and next-neighbour coupling require very high control over the coupling strengths to achieve any kind of degeneracy in the ground state (see Sec. 2.2.2). This is not very realistic in an experimental set-up, as it usually just collapses into the single-channel Kondo effect, as soon as the smallest asymmetries are introduced. The usual approach to overscreening is thus not a single lattice, but multiple ones [43–45]. In this thesis, the multiple-lattice set-up is referred to as *forced overscreening*. In Sec. 3.1 the theoretical background behind forced overscreening and in Sec. 3.2 the numerical results for an exemplary one-dimensional system are discussed.

3.1. Set-up

Given a system consisting of multiple independent lattices, with no hopping in between and non-zero coupling of each impurity spin to each lattice. An example system of this set-up with two lattices and a single impurity is illustrated in Fig. 3.1. It is important to emphasize that this set-up is possible with multiple impurities as well, even though the numerical discussions and example systems are limited to a single one. The resulting hopping matrix $t_{jj'}$ is composed of a matrix for each lattice in a block matrix form. The M lattices are numbered with the index $\mu \in \{1, \dots, M\}$. Diagonalizing the resulting unperturbed Hamiltonian H_0 thus results in a block diagonal diagonalization matrix U with M blocks. In general, one has M lattices and with possibly different Fermi Energies $k_F^{(\mu)}$ and thus there is an additional sum $\sum_{\mu=1}^M$ and index (μ) on each factor in Eq. (2.1.9). By repeating the analysis from Sec. 2.1 for each of the M summands, one finds the

3. Forced overscreening

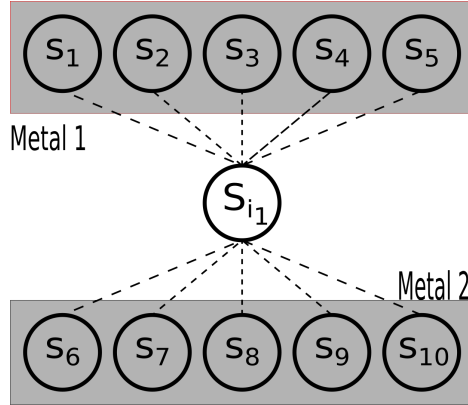


Figure 3.1.: Example for a system in which an impurity is forced to couple to at least two orbitals.

respective effective coupling spaces $\mathcal{H}_1^{(\mu)}$, and therefore, in total $\eta = \sum_{\mu=1}^M \dim \mathcal{H}_1^{(\mu)} \geq M$. Thus, by coupling an impurity spin to multiple independent lattices, it is possible to force M -channel overscreening. This kind of set-up will be referred to as *forced overscreening* from now on.

3.2. Numerical results

This Sec. is about the discussion of the calculation results for an exemplary forced overscreening set-up. The examined system consists of two one-dimensional lattices with open-boundary conditions (i.e. chains with loose ends), each with 49 sites and 25 conduction electrons. Like before, the two unperturbed lattices are governed by the tight-binding regime and the perturbation is given with isotropic next-neighbour coupling, with the same energy scales, i.e $t = 1$ (see beginning of Sec. 2.2). In between the two lattices is an impurity which couples symmetrically to a spin of each lattice with coupling strength J . This system is schematically pictured in Fig. 3.2(a) with its energy levels in Fig. 3.2(b), which are derived in Ref. [47]. This layout, of placing an impurity in between lattices, has been used in measurements [43] and theoretical discussions [39].

One sees that the symmetry of the system implies that the effective coupling constant to both lattices is the same, $\lambda_1 = \lambda_2 = \lambda$, since both lattices are physically equivalent. The result is a system similar to Fig. 3.1. The numerical calculation gives the expected

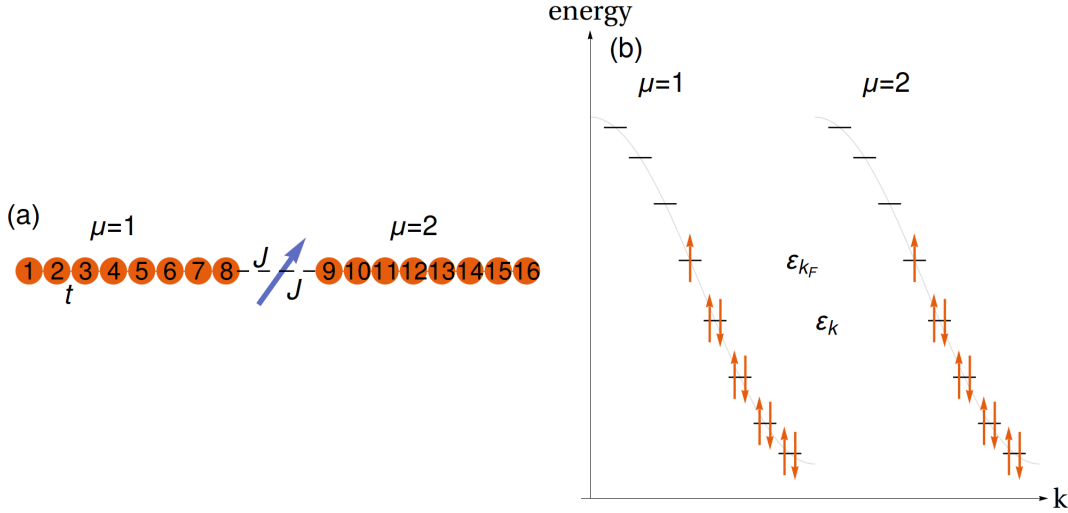


Figure 3.2.: (a) Illustration of two lattices with each $L = 8$ sites and hopping t . A single impurity spin, sitting in between the lattices, is coupling to the outer sites of the lattices. (b) Corresponding energy diagram with $N = 18$ conduction electrons, i.e. 9 in each lattice. This case corresponds to $G(k_F) = 2$, $\Gamma = 4, M = 2$ and two k_F electrons.

number of delocalized orbitals

$$\eta = \begin{cases} 2 & J_{nn} \neq 0, \\ 0 & J_{nn} = 0. \end{cases} \quad (3.2.1)$$

One thus recovers a central spin model with three spins. Using $\lambda_1 = \lambda_2 = \lambda$ and the notation derived in Sec. 2.2.2, one finds the eigenenergies

$$\varepsilon_0 = \frac{\lambda}{2}, \quad \varepsilon_1 = 0, \quad \varepsilon_2 = -\lambda. \quad (3.2.2)$$

For both $\lambda < 0$ and $\lambda > 0$, ε_1 is not the lowest energy, and it is thus ignored from now on, as it cannot be the ground state energy of the system. For the eigenvectors of ε_0 , one finds the same $|\varepsilon_0, i\rangle$ as before (see Sec. 2.2.2):

$$\begin{aligned} |\varepsilon_0, 1\rangle &= |1\rangle, \\ |\varepsilon_0, 2\rangle &= \frac{1}{\sqrt{3}}(|2\rangle + |3\rangle + |4\rangle), \\ |\varepsilon_0, 3\rangle &= \frac{1}{\sqrt{3}}(|5\rangle + |6\rangle + |7\rangle), \\ |\varepsilon_0, 4\rangle &= |8\rangle. \end{aligned}$$

3. Forced overscreening

For $|\varepsilon_2, i\rangle$, using Eqs. (2.2.8) and (2.2.9), one finds that

$$\begin{aligned}
 |\varepsilon_2, 1\rangle &= \frac{2}{\sqrt{6}}|2\rangle - \sqrt{\frac{1}{6}}|3\rangle - \sqrt{\frac{1}{6}}|4\rangle, \\
 &= \underbrace{\sqrt{\frac{1}{6}}(|\downarrow, \uparrow, \uparrow\rangle - |\uparrow, \downarrow, \uparrow\rangle)}_{\text{Singlet: IMP and CE1}} + \underbrace{\sqrt{\frac{1}{6}}(|\downarrow, \uparrow, \uparrow\rangle - |\uparrow, \uparrow, \downarrow\rangle)}_{\text{Singlet: IMP and CE2}}, \tag{3.2.3}
 \end{aligned}$$

$$\begin{aligned}
 |\varepsilon_2, 2\rangle &= -\sqrt{\frac{1}{6}}|5\rangle - \sqrt{\frac{1}{6}}|6\rangle + \frac{2}{\sqrt{6}}|7\rangle, \\
 &= \underbrace{\sqrt{\frac{1}{6}}(|\uparrow, \downarrow, \downarrow\rangle - |\downarrow, \uparrow, \downarrow\rangle)}_{\text{Singlet: IMP and CE1}} + \underbrace{\sqrt{\frac{1}{6}}(|\uparrow, \downarrow, \downarrow\rangle - |\downarrow, \downarrow, \uparrow\rangle)}_{\text{Singlet: IMP CE2}}. \tag{3.2.4}
 \end{aligned}$$

One thus recovers the entangled singlet states from Sec. 2.2.2, but with no preference for either channel, i.e. complete delocalization. Coming to the results of the calculation, one sees in Fig. 3.3(a), that the eigenenergies between $|m_{S_{\text{tot}}}| = 1.5$ and $|m_{S_{\text{tot}}}| = 0.5$ are equal to ε_0 in phase I and split up in phase II where the $|m_{S_{\text{tot}}}| = 0.5$ ground state energies correspond to ε_2 . Fig. 3.3(b) confirms this, as $S_{\text{tot}} = 1.5$ in phase I, i.e. the system is in the state $|\varepsilon_0, i\rangle$, and $S_{\text{tot}} = 0.5$ in phase IIa, i.e. the system is in the state $|\varepsilon_2, i\rangle$. The phase transition coincides with the transition of λ from negative to positive values. One can interpret this qualitatively using Appendix B. Negative λ favour ferromagnetic coupling and one observes the same quadruplet as in phase I of Sec. 2.2.2. Positive λ favour anti-ferromagnetic coupling, but instead of transitioning into an overscreening state through two phases as in Sec. 2.2.2, the system immediately reaches the case of perfectly delocalized entangled singlets, which is depicted in Fig. 2.6(c), corresponding to a level of delocalization that was not reachable with only one lattice.

To conclude this Sec., the name "forced overscreening" can be justified, as anti-ferromagnetic coupling directly implies that the impurity becomes overscreened with a two-fold degeneracy of the free spin.

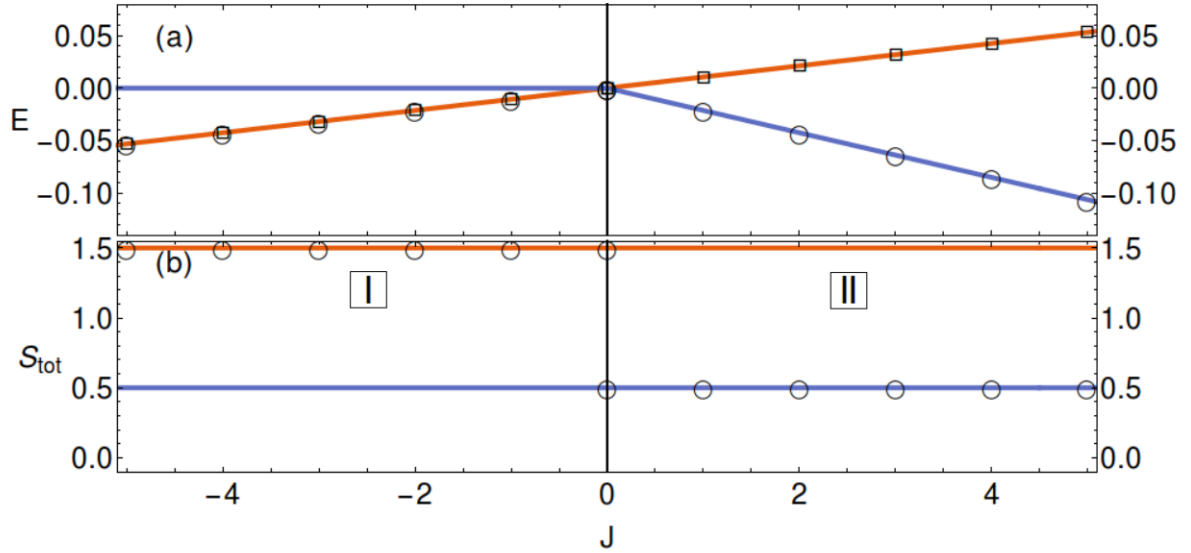


Figure 3.3.: Plots of various numerical results for two one-dimensional chains with loose ends each with $t = 1$, $L = 49$, $N = 50$ and varying next neighbour coupling strengths for the impurity in between the lattices J . Through (a)-(b), phase I is marked for negative J and phase II for positive J . (a) Plots of the ground state energies (arb. units). Numerical results for $|m_{S_{\text{tot}}}| = 0.5$ (1.5) are marked in circles (squares). Underlaid are the plots of the eigenenergy ε_2 (ε_0) in blue (red). (b) Plot of the electronic spin S_{tot} quantum number. Numerical results for $|m_{S_{\text{tot}}}| = 0.5$ are marked in circles. Underlaid are the plots of the quantum numbers S_{tot} to the expectation values $\langle \varepsilon_2, i | \mathbf{S}_{\text{tot}}^2 | \varepsilon_2, i \rangle$ in blue and to $\langle \varepsilon_0, i | \mathbf{S}_{\text{tot}}^2 | \varepsilon_0, i \rangle$ in red.

4. Conclusions and Outlook

A model, in which an arbitrary amount of magnetic impurities couple non-locally and anisotropically to conduction electron spins of a nanoscopic and metallic lattice with coupling strength J , has been examined. A linear-in- J perturbative approach was used. After applying a unitary transformation from real space to momentum space U and another unitary transformation V , a central spin model was recovered. In this model the impurities couple to η different effective delocalized conduction electron spins with the effective coupling strengths λ_i , whereby η is obtainable with the system's hopping matrix $t_{jj'}$ and coupling strength matrix J_{ni_r} . In the multi-impurity and multi-channel Kondo effect there are the three screening regimes under-, complete and overscreening. Using η it is possible to quickly form an expectation as to which screening regime to expect. This is a novelty of this model as in earlier works, in which only local coupling was considered, the possibility for overscreening was precluded. Using a sample of three systems, it was possible to show that overscreening does indeed occur, thus serving as a proof-of-concept that this formalism does describe the three screening regimes.

For the first two systems a one-dimensional ring lattice was used, which results in $\eta = 2$ for non-local coupling. For one k_F -electron the ground state is not degenerate and two phases have been identified. In the first phase the impurity couples ferromagnetically to one of the delocalized orbital spins, i.e. a triplet is formed. In the second phase the impurity couples anti-ferromagnetically to the other delocalized orbital spin, i.e. a singlet is formed. Non-degenerate complete screening is thus observed in phase II, even though there are two spin orbitals available. This is due to the fact, that the coupling constants are not equal and thus the orbital with the stronger coupling is prioritized.

Two phases were found in the two k_F -electron case. Phase I remains the phase with ferromagnetic coupling. The anti-ferromagnetic phase splits up into two regimes. In the first

4. Conclusions and Outlook

regime the impurity is not necessarily screened, because there is a probability that the two k_F -electrons form a singlet, rather than screening the impurity. The second regime corresponds to asymmetric overscreening. Asymmetric refers to the fact that while there are multiple screening channels, that completely screen the impurity with a two-fold degeneracy, the coupling constants λ_1, λ_2 are not equal. This raises the question whether different couplings in real space would lead to more delocalized singlet states, i.e. one could try to implement coupling with asymmetric next-neighbour constants, or enable next-nearest-neighbour coupling and evaluate these systems numerically. On the other hand, the fact that asymmetric two-channel coupling is preferred over single-channel coupling with the stronger orbital is a circumstance which deserves and requires explanation in and of itself.

The one-dimensional rings are systems with high symmetry, and one might have expected the coupling constants to the delocalized spin orbitals λ_i to be the same or at least to recover any other kind of symmetry in the effective model. Especially the case $J_{nn} \rightarrow \infty$, in which effectively two spin orbitals with symmetric coupling get mapped onto two orbitals with asymmetric coupling, is surprising. The question arises, at which point this symmetry is broken, and whether the breakdown of symmetry is generalizable to any system. If the breakdown of symmetry can be confirmed to contradict expectations, it might hint at shortcomings of the first-order perturbation theory and thus suggest an extension to the second-order. The evaluation of the second-order perturbative approach, as described in Ref. [46], might lead to interesting new insights, amongst other things because the "off-resonance" case (non-degenerate ground state or completely filled Fermi energy level) can only be described in the second-order.

In the one-dimensional forced overscreening system, i.e. an impurity between two one-dimensional chains with loose ends, one finds the immediate transition to the perfectly delocalized overscreening state for anti-ferromagnetic coupling, which was expected from previous measurement and discussions [39, 43]. As mentioned in Ref. [43], the accomplishment of overscreening requires fine-tuning of the coupling constants. If there is any asymmetry, the impurity will not form a singlet with the k_F -electrons from the weaker lattice and one ends up with effectively a single lattice. Experiments like the one in Ref. [43] show, that this level of fine-tuning is possible.

Forced overscreening also opens a plethora of set-up possibilities, just by connecting multiple lattices with multiple impurities in various ways, in which complicated competition regimes between under- and overscreening might occur, additionally to the competitions already known to arise in normal Kondo physics.

Having thoroughly discussed the one-dimensional case, it might prove more fruitful to move to higher dimensions. Especially because in one-dimensional systems the number of delocalized orbitals is limited to $\eta \leq 2$ per lattice (in the Kondo-Box, see Sec. 2). In two-dimensional systems η can be higher, and a topic of interest is, whether it is possible to fine-tune the coupling strengths J in such a way to manipulate η , i.e. transitioning through the various screening regimes just by varying the coupling strengths, possibly opening up possibilities for new and interesting systems. A foreboding to this could already be observed in the local case ($J_{nn} = 0$) in which $\eta \equiv 1$, so it is possible that less trivial changes of η might occur, but this would require further investigation.

Having seen that this extended formalism implies overscreening, one reaches the conclusion that the perturbative approach presented here is a capable description of each regime that occurs in Kondo physics (i.e. underscreening, complete screening and overscreening [34,37]) for finite lattices. It remains to show whether the results obtained from measurements are actually implied in this theory, which would be paramount to establishing this theory as a capable tool for description.

Another question that arises, is how the discussion of multichannel Kondo physics [39–43,45] can be combined with the discussion of multi-impurity Kondo physics [48–50]. For example analysing the RKKY interaction [28–30] for multi-impurity systems, as has been done in the local case in Ref. [32], with multiple orbitals $\eta > 1$, i.e. the relation of the orbitals for different impurities, might prove interesting and will be subject of future publications [33].

Another property that can be evaluated in the theory presented, but has been left out for simplicities sake, is anisotropic coupling of impurities to the lattice.

Finally the theory discussed here limits itself to the case of $T = 0$, or the low energy scale $T \ll \Delta E \ll T_K$ (with gap energy ΔE and Kondo temperature T_K), to focus on the description of the Kondo effect. For applicability, one would have to investigate the stability of the presented results in more realistic settings, by coupling the system to a

4. *Conclusions and Outlook*

bath for example. Especially states like the one obtained for $2k_F$ -electrons, in which there is an entangled state with asymmetric coupling, as discussed above, might be expected to collapse into single channel Kondo physics with the stronger orbital spin. Also, generalizing the discussion to include, for example, $\Delta E > T_K$ could give rise to interesting phase transitions which require further investigation.

A. One dimensional systems with periodic boundary conditions

In this App. the energy levels of a one dimensional system with periodic boundary conditions (i.e. a ring) in the tight-binding regime are derived. For that one has to diagonalize the hopping matrix on a lattice of length L with $n \in \{1, \dots, L\}$

$$\begin{aligned} H|n\rangle &:= t|n-1\rangle - t|n+1\rangle \\ &= t(U + U^\dagger)|n\rangle. \end{aligned}$$

One can rewrite this using the following unitary operator

$$U|n\rangle = |n-1\rangle,$$

which commutes with H . Now one proceeds to find the eigenvalues of U . Since it is unitary the eigenvalues are complex numbers of unitary value

$$U|\chi\rangle = e^{i\delta}|\chi\rangle.$$

Since $U^L = \mathbf{1}$, one gathers

$$e^{i\delta L} = 1 \quad \Rightarrow \quad \delta L = n2\pi \quad \Rightarrow \quad \delta = \delta_s = \frac{2\pi s}{L}, \quad s = 1, \dots, L.$$

Using this, one finds for the hopping matrix

$$H|\chi_s\rangle = 2t \cos(\delta_s)|\chi_s\rangle$$

and thus the result that the energy levels are two-fold degenerate, apart for the highest (for even lattice lengths) and lowest energy level.

B. Choosing the sign for the coupling constant

One generally wants to choose the sign for the coupling constant in such a way, that the anti-ferromagnetic case has the lower energy and is thus the ground state. Calculating the expectation value of the following Hamiltonian

$$\langle H_1 \rangle = J \langle \varphi | \mathbf{s} \mathbf{S} | \varphi \rangle ,$$

of a single impurity coupling to a single conduction electron with ladder operators, one finds

$$\langle H_1 \rangle = \left\langle \varphi \left| \frac{1}{2} (s^+ S^- + s^- S^+) + s_z S_z \right| \varphi \right\rangle ,$$

and from that the value of $\langle H_1 \rangle$ for the triplet

$$|\varphi\rangle \in \{ |\uparrow, \uparrow\rangle, |\downarrow, \downarrow\rangle, \frac{1}{\sqrt{2}} (|\uparrow, \downarrow\rangle + |\downarrow, \uparrow\rangle) \} ,$$

being $\langle H_1 \rangle_{\text{triplet}} = \frac{J}{4}$.

Analogously, one finds for the singlet $|\varphi\rangle = \frac{1}{\sqrt{2}} (|\uparrow, \downarrow\rangle - |\downarrow, \uparrow\rangle)$ an expectation value of $\langle H_1 \rangle_{\text{singlet}} = -\frac{3}{4}J$.

So positive J favour the anti-ferromagnetic case (i.e. the case where conduction electron spin and impurity spin are anti-parallel), which means it favours the case where screening can take effect.

Bibliography

- [1] WJ De Haas, J De Boer, and GJ Van den Berg. The electrical resistance of gold, copper and lead at low temperatures. *Physica*, 1(7-12):1115–1124, 1934.
- [2] Rudolf Gross and Achim Marx. *Festkörperphysik*. Walter de Gruyter GmbH & Co KG, 2014.
- [3] Jun Kondo. Resistance minimum in dilute magnetic alloys. *Progress of theoretical physics*, 32(1):37–49, 1964.
- [4] Alexander Cyril Hewson. *The Kondo problem to heavy fermions*, volume 2. Cambridge university press, 1997.
- [5] PW Anderson. A poor man’s derivation of scaling laws for the kondo problem. *Journal of Physics C: Solid State Physics*, 3(12):2436, 1970.
- [6] Kenneth G Wilson and John Kogut. The renormalization group and the ε expansion. *Physics Reports*, 12(2):75–199, 1974.
- [7] Philippe Nozieres. A “fermi-liquid” description of the kondo problem at low temperatures. *Journal of Low Temperature Physics*, 17(1-2):31–42, 1974.
- [8] N Andrei. Diagonalization of the kondo hamiltonian. *Physical Review Letters*, 45(5):379, 1980.
- [9] PB Wiegmann. Towards an exact solution of the anderson model. *Physics Letters A*, 80(2):163–167, 1980.
- [10] Ian Affleck. The kondo screening cloud: what it is and how to observe it. *arXiv preprint arXiv:0911.2209*, 2009.

Bibliography

- [11] Philip Warren Anderson. Localized magnetic states in metals. *Physical Review*, 124(1):41, 1961.
- [12] JR Schrieffer and PA Wolff. Relation between the anderson and kondo hamiltonians. *Physical Review*, 149(2):491, 1966.
- [13] David Goldhaber-Gordon, Hadas Shtrikman, D Mahalu, David Abusch-Magder, U Meirav, and MA Kastner. Kondo effect in a single-electron transistor. *Nature*, 391(6663):156–159, 1998.
- [14] Leo Kouwenhoven and Leonid Glazman. Revival of the kondo effect. *Physics world*, 14(1):33, 2001.
- [15] Michael Pustilnik and Leonid Glazman. Kondo effect in quantum dots. *Journal of Physics: Condensed Matter*, 16(16):R513, 2004.
- [16] Maxim Dzero, Kai Sun, Victor Galitski, and Piers Coleman. Topological kondo insulators. *Physical review letters*, 104(10):106408, 2010.
- [17] Xiaohang Zhang, NP Butch, P Syers, S Ziemak, Richard L Greene, and Johnpierre Paglione. Hybridization, inter-ion correlation, and surface states in the kondo insulator smb 6. *Physical Review X*, 3(1):011011, 2013.
- [18] FW Smith. Critical magnetic fields of a kondo superconductor: Znmn. *Journal of Low Temperature Physics*, 5(6):683–699, 1971.
- [19] Wolfgang B Thimm, Johann Kroha, and Jan von Delft. Kondo box: A magnetic impurity in an ultrasmall metallic grain. *Physical review letters*, 82(10):2143, 1999.
- [20] PS Cornaglia and CA Balseiro. Kondo impurities in nanoscopic systems: Confinement-induced regimes. *Physical Review B*, 66(11):115303, 2002.
- [21] Yan Luo, Claudio Verdozzi, and Nicholas Kioussis. Tunable doniach phase diagram for strongly-correlated nanoclusters. *Physical Review B*, 71(3):033304, 2005.
- [22] Thomas Hand, Johann Kroha, and Hartmut Monien. Spin correlations and finite-size effects in the one-dimensional kondo box. *Physical review letters*, 97(13):136604, 2006.

- [23] DC Ralph, CT Black, and M Tinkham. Spectroscopic measurements of discrete electronic states in single metal particles. *Physical review letters*, 74(16):3241, 1995.
- [24] DC Ralph, CT Black, and M Tinkham. Gate-voltage studies of discrete electronic states in aluminum nanoparticles. *Physical review letters*, 78(21):4087, 1997.
- [25] Corwin H Booth, Marc D Walter, Million Daniel, Wayne W Lukens, and Richard A Andersen. Self-contained kondo effect in single molecules. *Physical review letters*, 95(26):267202, 2005.
- [26] Teri W Odom, Jin-Lin Huang, Chin Li Cheung, and Charles M Lieber. Magnetic clusters on single-walled carbon nanotubes: the kondo effect in a one-dimensional host. *Science*, 290(5496):1549–1552, 2000.
- [27] Yu Bomze, I Borzenets, H Mebrahtu, A Makarovski, HU Baranger, and G Finkelstein. Two-stage kondo effect and kondo-box level spectroscopy in a carbon nanotube. *Physical Review B*, 82(16):161411, 2010.
- [28] Melvin A Ruderman and Charles Kittel. Indirect exchange coupling of nuclear magnetic moments by conduction electrons. *Physical Review*, 96(1):99, 1954.
- [29] Tadao Kasuya. A theory of metallic ferro-and antiferromagnetism on zener’s model. *Progress of theoretical physics*, 16(1):45–57, 1956.
- [30] Kei Yosida. Magnetic properties of cu-mn alloys. *Physical Review*, 106(5):893, 1957.
- [31] Andrej Schwabe, Daniel Gütersloh, and Michael Potthoff. Competition between kondo screening and indirect magnetic exchange in a quantum box. *Physical review letters*, 109(25):257202, 2012.
- [32] Andrej Schwabe, Mirek Hänsel, Michael Potthoff, and Andrew K Mitchell. Screening mechanisms in magnetic nanostructures. *Physical Review B*, 92(15):155104, 2015.
- [33] Mirek Hänsel and Michael Potthoff. (unpublished). Will deal with multi-impurity effects in non-local coupling problems, 2016.

Bibliography

- [34] Ph Nozières and A Blandin. Kondo effect in real metals. *Journal de Physique*, 41(3):193–211, 1980.
- [35] N Andrei and C Destri. Solution of the multichannel kondo problem. *Physical review letters*, 52(5):364, 1984.
- [36] Ian Affleck and Andreas WW Ludwig. Exact conformal-field-theory results on the multichannel kondo effect: Single-fermion green’s function, self-energy, and resistivity. *Physical Review B*, 48(10):7297, 1993.
- [37] DL Cox and A Zawadowski. Exotic kondo effects in metals: magnetic ions in a crystalline electric field and tunnelling centres. *Advances in Physics*, 47(5):599–942, 1998.
- [38] Andrew K Mitchell, Eran Sela, and David E Logan. Two-channel kondo physics in two-impurity kondo models. *Physical review letters*, 108(8):086405, 2012.
- [39] S Di Napoli, A Weichselbaum, P Roura-Bas, AA Aligia, Y Mokrousov, and S Blügel. Non-fermi-liquid behavior in transport through co-doped au chains. *Physical review letters*, 110(19):196402, 2013.
- [40] A Altland, B Béri, R Egger, and AM Tsvelik. Multichannel kondo impurity dynamics in a majorana device. *Physical review letters*, 113(7):076401, 2014.
- [41] KT Law, CY Seng, Patrick A Lee, and TK Ng. Quantum dot in a two-dimensional topological insulator: The two-channel kondo fixed point. *Physical Review B*, 81(4):041305, 2010.
- [42] Maxim Kharitonov and Gabriel Kotliar. Kondo effect in monolayer and bilayer graphene: Physical realizations of the multichannel kondo models. *Physical Review B*, 88(20):201103, 2013.
- [43] RM Potok, IG Rau, Hadas Shtrikman, Yuval Oreg, and D Goldhaber-Gordon. Observation of the two-channel kondo effect. *Nature*, 446(7132):167–171, 2007.
- [44] Sheng-Shiuan Yeh and Juhn-Jong Lin. Two-channel kondo effects in al/alo x/sc planar tunnel junctions. *Physical Review B*, 79(1):012411, 2009.

- [45] LJ Zhu, SH Nie, P Xiong, P Schlottmann, and JH Zhao. Orbital two-channel kondo effect in epitaxial ferromagnetic 110-mnml films. *Nature communications*, 7, 2016.
- [46] Fabian HL Essler, Holger Frahm, Frank Göhmann, Andreas Klümper, and Vladimir E Korepin. *The one-dimensional Hubbard model*. Cambridge University Press, 2005.
- [47] Devadatta Kulkarni, Darrell Schmidt, and Sze-Kai Tsui. Eigenvalues of tridiagonal pseudo-toeplitz matrices. *Linear Algebra and its Applications*, 297(1):63–80, 1999.
- [48] NJ Craig, JM Taylor, EA Lester, CM Marcus, MP Hanson, and AC Gossard. Tunable nonlocal spin control in a coupled-quantum dot system. *Science*, 304(5670):565–567, 2004.
- [49] Lihui Zhou, Jens Wiebe, Samir Lounis, Elena Vedmedenko, Focko Meier, Stefan Blügel, Peter H Dederichs, and Roland Wiesendanger. Strength and directionality of surface ruderman–kittel–kasuya–yosida interaction mapped on the atomic scale. *Nature Physics*, 6(3):187–191, 2010.
- [50] N Néel, R Berndt, J Kröger, TO Wehling, AI Lichtenstein, and MI Katsnelson. Two-site kondo effect in atomic chains. *Physical review letters*, 107(10):106804, 2011.

Acknowledgments

I acknowledge the very insightful and fruitful discussions with Michael Potthoff and Mirek Hänsel and wish to thank them for the continued support and helpfulness. I also wish to thank Tom Weber for the discussions we had.

Statement under oath

Hiermit bestätige ich, dass die vorliegende Arbeit von mir selbständig verfasst wurde und ich keine anderen als die angegebenen Hilfsmittel – insbesondere keine im Quellenverzeichnis nicht benannten Internet-Quellen – benutzt habe und die Arbeit von mir vorher nicht einem anderen Prüfungsverfahren eingereicht wurde. Die eingereichte schriftliche Fassung entspricht der auf dem elektronischen Speichermedium. Ich bin damit einverstanden, dass die Bachelorarbeit veröffentlicht wird.

Hamburg, 2. September 2018,